Characterization of the material response in granular ratcheting

R. García-Rojo,* F. Alonso-Marroquín, and H. J. Herrmann
ICP, University of Stuttgart, Pfaffenwaldring 27, 70569 Stuttgart, Germany
(Received 20 May 2005; published 10 October 2005)

The existence of a very special ratcheting regime has recently been reported in a granular packing subjected to cyclic loading. In this state, the system accumulates a small permanent deformation after each cycle. The value of this permanent strain accumulation becomes independent of the number of cycles after a short transient regime. We show in this paper that a characterization of the material response in this peculiar state is possible in terms of three simple macroscopic variables. The definition of these variables is such that they can be easily measured both in the experiments and in the simulations. A thorough investigation of the micro- and macromechanical factors affecting these variables has been carried out by means of molecular-dynamics simulations of a polydisperse disk packing, as a simple model system for granular material. Biaxial test boundary conditions with periodically varying load were implemented. The effect on the plastic response of the confining pressure, the deviatoric stress, and the number of cycles has been investigated. The stiffness of the contacts and friction has been shown to play an important role in the overall response of the system. Especially illustrative is the influence of the peculiar hysteretical behavior in the stress-strain space on the accumulation of permanent strain and the energy dissipation.

DOI: 10.1103/PhysRevE.72.041302 PACS number(s): 45.70.Cc, 61.43.Bn

I. INTRODUCTION

Brownian motors, quantum ratchets, or molecular pumps operate under the same principle: The chaos of the microworld cannot be avoided, but one can take advantage of it [2]. Nanoscale ratchet devices have been designed with the surprising property that they can extract work from the noise of thermal and quantum fluctuations [3]. Ratcheting is the mechanism behind molecular motors, which can use the chaotic Brownian motion to turn directionless energy into directed motion [4]. These lilliputian motors seem to be responsible for many biological process, such as mechanical transport [5] or muscle contraction [6]. Apart from these fascinating machines, the ratchet effect has been used to describe economical or sociological processes in which the intrinsic asymmetry in the system allows us to rectify an unbiased input [7]. A ratchetlike effect is also the major cause of material deterioration due to cyclic stress loading and thermal or mechanical fluctuations [8–10]. Asymmetries in foundations can produce tilting and eventual collapse of any structure due to ratcheting [11]. The tower of Pisa is a well documented case, where the tilt was observed from its construction in 1173 [12]. Pavement design is another important field in which graded soils are used as supportive roadbed [8,13–15]. The excitations that traffic imposes on the sublayer produce deformations in the granular material. These deformations are transmitted to the upper layers of the pavements, causing its degradation or even its breakage. Cyclic loading tests are extensively used in the investigation of the plastic response of unbound granular matter [13]. In these experiments, the material is subjected to a certain cyclic stress condition mimicking traffic. From a practical point of view, the main question is whether the material accumulates plastic deformation in each cycle, or whether it adapts to the excitation reaching a shakedown state. Only materials in which the excitations *shake down* should be consequently used in pavement design.

The use of simple models of granular materials allows the numerical solution of the dynamics. Discrete element methods (DEM) such as molecular dynamics (MD) [16–18] and contact dynamics (CD) [19,20] have been in fact often successfully applied to the investigation of the elastoplastic behavior of granular matter. Especially interesting from the physical point of view is how the contact model affects the overall response [21,22]. Recent MD results have shown the key role that sliding plays on the plastic deformation of a granular packing subjected to cyclic loading, and the existence of a range of values of the excitations for which a simple viscoelastic model of disks subjected to cyclic loading attains shakedown [1,23]. Beyond the shakedown limit, two other possible responses have also been identified: For very high loads, the material accumulates deformations at a relatively high constant rate, leading to an incremental collapse of the structure; for moderate loading intensities, the system undergoes an adaptation process in which the accumulation of deformation gradually decreases to a very low constant value. This post-compaction is associated with a relaxation of the dissipated energy per cycle, which progressively decreases to a constant value dependent on the imposed loading. In this final stage, there is a small but persistent accumulation of permanent strain, associated with a periodic behavior of the sliding contacts, which is called the ratcheting regime [1].

Due to the nonlineality and the irreversibility of the behavior, cyclic loading is a rather complicated problem from the theoretical point of view. Elastoplastic and hypoplastic theories can account for the change in the incremental stiffness during loading and unloading phases, only if basic modifications are undertaken [24,25]. In the case of elasto-

*URL: http://www.icp.uni-stuttgart.de/~rojo; Electronic address: rojo@icp.uni-stuttgart.de

plasticity, the overall plastic behavior in the loading-unloading is obtained as the result of a combination of several *yield surfaces* [26]. In the hypoplastic theory, the *intergranular strain* is introduced to take into account the dependence of the response on the deformation history [27]. Interestingly, a point of convergence of both theories has been established by the *bounding surface elastoplasticity* [28]. This theory introduces a tiny elastic nucleus changing with the deformation, and describe the hysteresis by means of internal variables taking into account the evolution of the microstructure. The characterization of such internal variables has been traditionally done using structure tensors, measuring the fabric properties of the contact network [29]. There is numerical evidence that a single fabric tensor, measuring the anisotropy of the contact network, can be used to characterize the resilient response [30]. But the description of the plastic deformation requires taking into account the inherent decomposition of the contact network in sliding and nonsliding contacts [31]. The role of kinematic modes such as sliding and rolling has also been investigated to some extent for monotonic deformation, but not for cyclic loading [16,32,33].

The final aim of this paper is the characterization of the ratcheting response of a granular packing under cyclic loading. For this purpose, three macroscopic variables will be introduced. A simple DEM model will then be used to investigate the dependence of the material response on different macroscopic and microscopic variables. From this investigation, we have found that our simple model is able to reproduce several behaviors observed in the experience, and microscopically justifies the use of popular empirical laws, such as the k-θ model. The main parameters of our model and the details of the MD simulations are presented in Sec. II. The ratcheting regime resulting in the biaxial test is described in Sec. III. In Sec. IV, we decompose the strain response in its permanent and resilient components. We continue with an analysis of hysteresis in the plastic response, establishing in Sec. V a direct relation between the particular shape of the stress-strain cycle and the dissipated energy per cycle. From this relationship, it will be easy to explain the observed dependence of the dissipated energy per cycle on the deviatoric stress. Results on the permanent strain and the resilient parameters are presented for the different cases studied in Secs. VI and VII. The approach proposed here is basically empirical. The resilient parameters will be therefore conveniently defined in terms of the recoverable deformation, as is usually done by experimentalists [34]. The dependence on the imposed stress is investigated, and the results are compared to predictions of resilient response models [35–38]. The influence of the friction and the stiffness at the contacts, main micromechanical parameters of the model, will also be determined. We finish in Sec. VIII with a discussion of the main conclusions of this work.

II. MODEL

In our viscoelastic 2D model, the grains are modeled by soft disks. The deformation that two grains suffer during the interaction is reproduced by allowing that the disks overlap. During the overlapping, a certain force f^c is exerted at the contact point. This force can be decomposed in the following parts:

$$\vec{f}^c = \vec{f}^e + \vec{f}^v, \tag{1}$$

where $\vec{f}^e$ and $\vec{f}^v$ are the elastic and the viscous contribution, respectively. The elastic part of the contact force is also decomposed as

$$f^e = f_n^e \hat{n}^c + f_t^e \hat{t}^c. \tag{2}$$

The unit normal vector $\hat{n}^c$ points in the direction of the vector connecting the center of mass of the two disks. The tangential vector $\hat{t}^c$ is perpendicular to $\hat{n}^c$. The normal elastic force is calculated as

$$f_n^e = -k_n A/L_c, \tag{3}$$

where k_n is the normal stiffness, A is the overlapping area, and L_c is a characteristic length of the contact. Our choice is $L_c = R_i + R_j$. This normalization is necessary to be consistent in the units of force.

In our simulations, we will assume Coulomb friction. This model introduces a static and a sliding tangential force, $F_s = \mu_s F_n$ and $F_d = \mu_d F_n$, respectively, in terms of the static, μ_s, and dynamic, μ_d, friction coefficients. Since the coefficients satisfy the relation $\mu_d < \mu_s$, there is a nonsmooth transition from the nonsliding to the sliding condition, which cannot be captured by the molecular-dynamics scheme. A regularization process is usually assumed implying that $\mu_s = \mu_d = \mu$ in order to overcome this drawback and implement coulomb friction in DEM quasistatic simulations [53].

At each contact, the force is calculated using an extension of the method proposed by Cundall-Strack [39]. This is a well established simple model suitable for the simulation of quasistatic deformation of granular materials [52]. An elastic force proportional to the elastic displacement is included at each contact,

$$f_t^e = -k_t \Delta x_t^e, \tag{4}$$

where k_t is the tangential stiffness. The elastic displacement Δx_t is calculated as the time integral of the tangential velocity of the contact during the time where the elastic condition $|f_t^e| < \mu f_n^e$ is satisfied. The sliding condition is imposed, keeping this force constant when $|f_t^e| = \mu f_n^e$. The straightforward calculation of this elastic displacement is given by the time integral starting at the beginning of the contact,

$$\Delta x_t^e = \int_0^t v_t^c(t') \Theta(\mu f_n^e - |f_t^e|) dt', \tag{5}$$

where Θ is the Heaviside step function and $\vec{v}_t^c$ denotes the tangential component of the relative velocity $\vec{v}^c$ at the contact,

$$\vec{v}^c = \vec{v}_i - \vec{v}_j + \vec{\omega}_i \times \vec{R}_i - \vec{\omega}_j \times \vec{R}_j. \tag{6}$$

Here $\vec{v}_i$ is the velocity and $\vec{\omega}_i$ is the angular velocity of the particles in contact. The branch vector $\vec{R}_i$ connects the center of mass of particle i to the point of application of the contact force. Replacing Eqs. (3) and (4) into Eq. (2), one obtains

$$\vec{f}^e = -k_n \frac{A}{L_c} \hat{n}^c - k_t \Delta x_t^e \hat{t}^c. \quad (7)$$

Damping forces are included in order to allow rapid relaxation during the preparation of the sample, and to reduce the acoustic waves produced during the loading. These forces are calculated as

$$\vec{f}^v = -m(\gamma_n v_n^c \hat{n}^c + \gamma_t v_t^c \hat{t}^c), \quad (8)$$

where $m=(1/m_i+1/m_j)^{-1}$ is the effective mass of the disks in contact. $\hat{n}^c$ and $\hat{t}^c$ are the normal and tangential unit vectors defined before, and γ_n and γ_t are the coefficients of viscosity. These forces introduce time-dependent effects during the loading. However, these effects can be arbitrarily reduced by increasing the loading time, as corresponds to the quasistatic approximation.

The interaction of the disks with the walls is modeled by using a simple viscoelastic force: First, we allow the disks to penetrate the walls. Then we include a force

$$\vec{f}^b = -(k_n \delta + \gamma_b m_\alpha v^b)\vec{n}, \quad (9)$$

where δ is the penetration length of the disk, $\vec{n}$ is the unit normal vector to the wall, and v^b is the relative velocity of the disk with respect to the wall.

The evolution of the position $\vec{x}_i$ and the orientation φ_i of the particle i is governed by the equations of motion

$$m_i \ddot{\vec{x}}_i = \sum_c \vec{f}_i^c + \sum_b \vec{f}_i^b,$$

$$I_i \ddot{\varphi}_i = \sum_c \vec{R}_i^c \times \vec{f}_i^c + \sum_b \vec{R}_i^b \times \vec{f}_i^b. \quad (10)$$

Here m_i and I_i are the mass and moment of inertia of the disk. The first sum goes over all those particles in contact with this particle, the second one over all the contacts of i with the walls. The interparticle contact forces are given by replacing Eqs. (7) and (8) in Eq. (1).

We use a fifth-order Gear predictor-corrector method for solving the equation of motion [40]. This algorithm consists of three steps. The first step predicts position and velocity of the particles by means of a Taylor expansion. The second step calculates the forces as a function of the predicted positions and velocities. The third step corrects the positions and velocities in order to optimize the stability of the algorithm. This method is much more efficient than the simple Euler approach or the Runge-Kutta method, especially for cyclic loading, where very high accuracy is required.

The relevant contact parameters of this model are the normal stiffness at the contacts k_n, the ratio of tangential and normal stiffness k_t/k_n, the normal and tangential damping frequencies, and the friction coefficient. In the quasistatic approximation, the results are independent of the frequency of the cyclic loading and the damping constants. The system is polydisperse, being that the radii of the grains are Gaussian distributed with a mean value of $0.1L_0$ and a variance of 0.36, where L_0 is the original length of the biaxial box.

III. ONSET OF GRANULAR RATCHETING

In a biaxial experiment, the sample is subjected to a certain stress state characterized by the principal stresses σ_1 and σ_2. In this case, the stress space is therefore a plane, since the third component is zero, $\sigma_3 \equiv 0$. In our simulations, the system is first homogeneously compressed with $\sigma_1=\sigma_2$. After an equilibrium state under the pressure $P_0=(\sigma_1+\sigma_2)/2=\sigma_1$ has been reached, the vertical stress is quasistatically changed,

$$\sigma_2(t) = P_0 \left\{ 1 + \frac{\Delta\sigma}{2} \left[1 - \cos\left(\frac{2\pi t}{t_0} \right) \right] \right\}, \quad (11)$$

where t is the simulation time and t_0 is the period of the loading. Note that $\Delta\sigma$, introduced in the last equation, is the maximum deviatoric stress measured in units of P_0. In our approximation, it fully characterizes the intensity of the cyclic load imposed on the walls.

Deformation appears in the sample due to the imposed excitations. The strain is the magnitude that characterizes the accumulation of permanent deformation in the sample. Among the different practical definitions of strain available [41], we have chosen Cauchy's definition, which is basically the ratio of the new and the original length of the system. Let L_0^i be the original length of the sample in the principal direction i $(i=x,y)$. The principal component of the strain tensor ϵ_{ij} on this direction will then be

$$\epsilon_i(t) \equiv \epsilon_{ii}(t) = \frac{L_i(t) - L_0^i}{L_0^i}, \quad (12)$$

where L_i is the length of the system in the principal direction i at the moment of the measurement.

Different loading intensities will be exerted on the sample by changing the value of $\Delta\sigma$. The reaction of the system will be characterized by the deviatoric permanent strain, γ, that is the difference between the strains in the principal directions,

$$\gamma = \epsilon_2 - \epsilon_1. \quad (13)$$

The typical evolution of the permanent strain during the cyclic loading is shown in Fig. 1 for our 400-particle model system. The stress-strain relation consists of hysteresis loops. This hysteresis produces an accumulation of deviatoric strain with the number of cycles in addition to a progressive compaction, which is not shown there. After some decades of cycles, the accumulation of permanent deformation becomes linear, as shown in Fig. 2. This strain rate remains constant for a very large number of cycles, even when the volume ratio is very close to the saturation level.

A micromechanical explanation of this linear accumulation of strain is provided by following the dynamics of the contact network. Although most of the contact forces of this network satisfy the elastic condition $|f_t| < \mu f_n$, the strong heterogeneities produce a considerable amount of contacts reaching the sliding condition $|f_t| = \mu f_n$ during the compression. After a number of loading cycles, the contact network reaches a quasiperiodic behavior. In this regime, a fraction of the contacts reaches almost periodically the sliding condition, as shown in the inset of Fig. 2. In each load-unload transition there is an abrupt reduction of sliding contacts, which induces the typical discontinuity of the stiffness upon

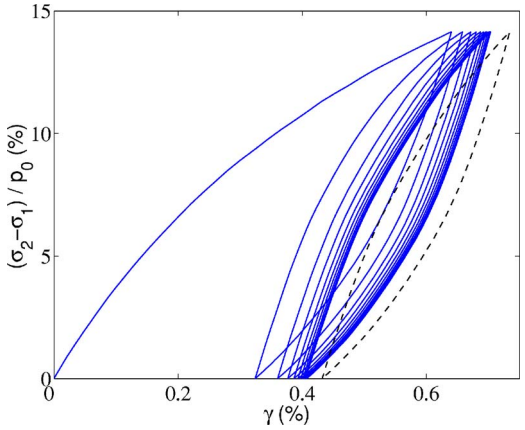

FIG. 1. (Color online) Typical stress-strain relation during cyclic loading. In the long-time behavior, the response is given by a limit hysteresis loop. This is shown by the dashed line (the loop here corresponds to the cycle $N=1000$). In this simulation, $\Delta\sigma=0.14P_0$ and $P_0=10^{-4}k_n$, where the normal contact stiffness is $k_n=2\times10^6$ N/m. The damping constants are defined in terms of the characteristic oscillation period $t_s=\sqrt{k_n/\rho\lambda^2}$ (in our case, $t_s=0.1414$), where ρ is the density of the grains and λ is the mean radius of the disks composing the sample. The period of oscillation was taken long enough ($t_0=10^5t_s$) to be sure that we are in the quasistatic limit.

reversal of the loading. The load-unload asymmetry at each sliding contact causes it to slip the same amount and in the same direction during each loading cycle, leading to an overall ratcheting response.

The contact behavior can be observed by embedding two points at each particle near to the contact area, and following their translation during each cycle. Their relative displacements are calculated as $\vec{s}^i=\vec{s}_0-\vec{s}_{\mathrm{rb}}$, where $\vec{s}_0$ is the displacement of the embedded point i and $\vec{s}_{\mathrm{rb}}$ is the rigid-body motion. This latter is given by the vector connecting the initial to the final position of the contact point. Note that $\vec{s}=\vec{0}$ when the two particles move as a rigid body.

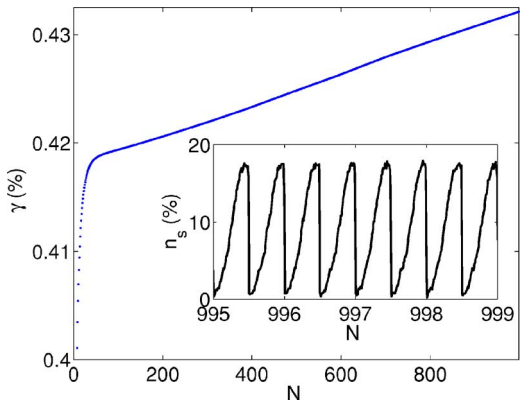

FIG. 2. (Color online) Cumulative permanent deformation against the number of cycles (N). After the post-compaction regime, the system accumulates permanent strain at a constant strain rate. This is the so-called ratcheting regime, which emerges as a result of the periodicity of the sliding contacts. The inset shows precisely the fraction of the sliding contact vs time in this state.

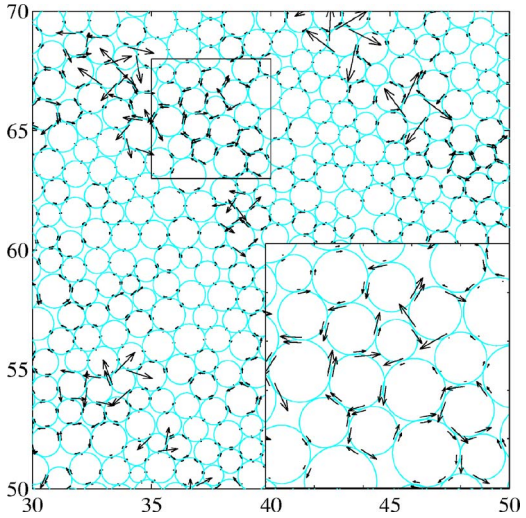

FIG. 3. (Color online) Displacement at the contacts during one cycle in the ratcheting. The arrows are proportional to the displacements s of the two material points at the contacts referred to the contact point. More details are found in the text. The figure is a snapshot of the simulation of Fig. 1 for $N=1000$.

Figure 3 shows the displacement at the contacts during cycle $N=1000$. Simulations show that, in this regime, this displacement field is almost constant after each cycle. There are two deformation modes resembling the mechanical ratchets. (i) At the sliding contacts the displacement vectors do not agree, so that there is a systematic slip during each cycle which also leads to a constant frictional dissipation per cycle. (ii) At the nonsliding contacts, the displacement vectors are almost the same for the two particles.

Note from Fig. 3 that the distribution of these ratchets is not uniform. This kind of strain localization with intense rolling is typical in sheared granular materials [32,42]. Fundamental differences are, however, observed between the cyclic loading response and the behavior under monotonic shear: The translation of each particle during the ratcheting regime is given by an almost constant displacement per cycle. On the other hand, the displacement of the particle during monotonic shear is rather chaotic, well described by an anomalous diffusion [43].

Such systematic translation per cycle of the individual grains in the ratcheting regime has a strong spatial correlation. This is shown in the displacement field of Fig. 4. The most salient feature here is the formation of vorticity cells, where a cluster of particles rotates as a whole. These vorticities survive during several hundred cycles, contrary to the simple shear case, where the vorticities have a very short lifetime [43]. It is interesting to see, from Figs. 3 and 4, the kinematic phase separation of the grains: (a) Grains organized in large vorticity cells, and (b) grains which accommodate the cells to make them more compatible with the imposed boundary conditions. Since such kinematic modes are linked with the nonvanishing antisymmetric part of the displacement gradient, the strain tensor is not sufficient to provide a complete description of this convective motion during cyclic loading. An appropriate continuum description of ratcheting would require additional continuum variables tak-

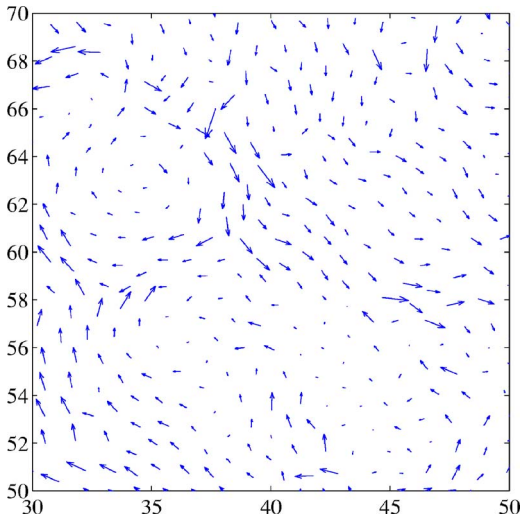

FIG. 4. (Color online) Vortex formation as a consequence of the ratcheting of the particles. The arrows are proportional to the displacement of the particle after one cycle in the ratcheting regime. They are plotted at the center of the disks. The cycle is the same as the one shown in Fig. 3.

ing into account the vorticity and the gearing between the contacts. As in the case of the shear band formation, the Cosserat theory may be a good alternative [44].

IV. MATERIAL RESPONSE TO CYCLIC LOADING

The existence of an elastic region in the deformation of granular materials implies that there is a finite region in the space of stress states around the origin, in which the system reacts reversibly. Experiments and simulations show, however, that there is not such pure elastic behavior in a granular sample. This is not in contradiction with the existence of shakedown: A granular system may not accumulate any systematic permanent deformation after one loading cycle, but will always dissipate some energy because grain interactions are inherently inelastic. This is possible thanks to the additional energy supplied to the system by the external loading. In the particular case of our model, the system reaches a viscoelastic shakedown. In this limit state, the system dissipates some energy in each cycle and the overall behavior is not elastic, but the stress-strain cycle is still hysteretic (see Fig. 5). Therefore, we differentiate in cyclic loading between an elastic and a resilient deformation of the sample. The latter implying that no permanent deformation has been accumulated after one cycle, while the first also implies the total absence of hysteresis or memory effects in the response.

It has been recently shown that there is a broad range of values of $\Delta\sigma$ for which a granular packing reacts to the imposed cyclic excitations by slowly deforming in a ratcheting regime [1,23]. This is a quasiperiodic state, macroscopically characterized by a constant strain rate and a conservation of the shape of the stress-strain cycle (see Fig. 1). At the beginning of the loading process, the system suffers a rearrangement of the sliding contacts, after which they start to behave periodically within the loading cycles. This *post-compaction*

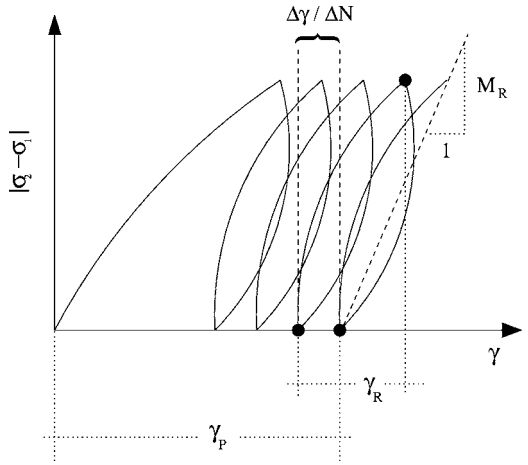

FIG. 5. Sketch of the typical material reaction to cyclic loading in the granular ratcheting. After a post-compaction stage, the system accumulates permanent strain, γ_P, at a constant strain rate $\Delta\gamma/\Delta N$. The resilient modulus M_R is also indicated, as defined in Eq. (14).

process is associated with a relaxation of the strain rate and also of the dissipated energy per cycle toward a constant value [23]. This stationary value of the strain rate fully determines the macroscopic plastic response of the system in the ratcheting regime. At any stage of the experiment, the strain can therefore be decomposed in two well differentiated components. The irreversible plastic strain accumulated after the end of the current cycle, γ_P, and the recoverable resilient strain, γ_R, accumulated along the cycle. In the ratcheting regime, the strain rate $(\Delta\gamma/\Delta N)$ is approximately constant, while the latter deformation is well characterized by the resilient parameters: resilient modulus M_R and the Poisson ratio ζ. The first parameter, as it appears in Fig. 5, is the ratio of the maximum deviatoric stress and the corresponding deviatoric resilient strain,

$$M_R = \frac{\Delta\sigma}{\gamma_R}, \tag{14}$$

and quantifies the overall stiffness of the material. The Poisson ratio, correspondingly, is the ratio of the horizontal (ϵ_1^R) and axial (ϵ_2^R) resilient strains,

$$\zeta = -\frac{\epsilon_1^R}{\epsilon_2^R}. \tag{15}$$

It measures how isotropic the deformation is. The definition of ϵ_1^R and ϵ_2^R is similar to that in Eq. (12). They are both measured at the final stage of the loading, just before unloading starts. Similarly to Eq. (13), the resilient deviatoric strain is defined in terms of the resilient strains as $\gamma^R = \epsilon_2^R - \epsilon_1^R$.

As a consequence of the quasistatic change of the stresses, all the relevant time dependence occurs in the system through the number of cycles N. Figure 6 shows the evolution of the resilient parameters from the simulations for different deviatoric stresses. For low excitations, the curves have already reached a *plateau* after a couple of cycles, implying that the values of ζ and M_R do not apparently change as the number of cycles increases. In the initial post-

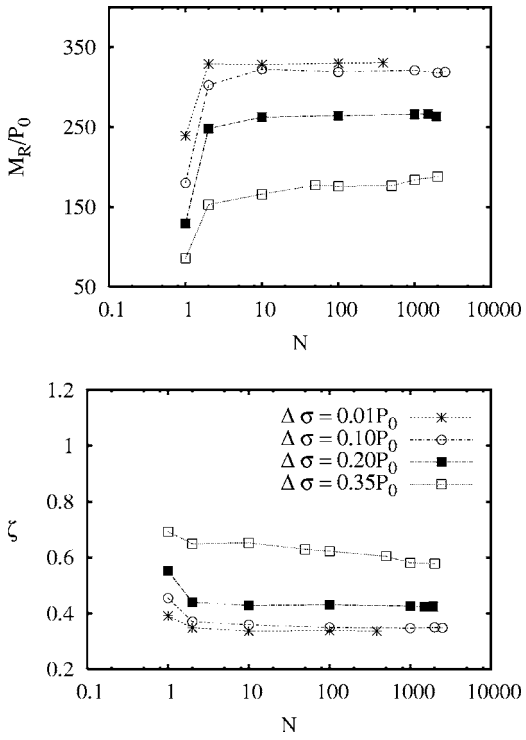

FIG. 6. Evolution of the resilient parameters with the number of cycles N: Resilient modulus M_R (top) and Poisson ratio ζ (bottom). The curves show the measures of these magnitudes for different values of the deviatoric stress $\Delta\sigma$. The data in the figure correspond to the simulation of a system with 400 disks, friction coefficient $\mu=0.1$, normal stiffness $k_n=2\times10^6$ N/m, normal damping $1/\gamma_n=4\times10^2 t_s$, and tangential damping $1/\gamma_t=8\times10^1 t_s$. The confining pressure here is $P_0=6\times10^{-4}k_n$.

compaction stage, the system accumulates more deviatoric strain in the horizontal direction (perpendicular to the direction on which the cyclic load is applied) than it does in the final stage. This explains why the Poisson ratio decreases slightly in the first cycles. The resilient modulus increases, however, implying a higher stiffness of the system after the post-compaction. Although the dependence of the final values on the imposed loading will be discussed in a latter section of this paper, it should now be remarked that the number of cycles needed for the system to reach a steady resilient response increases as the imposed deviatoric stress is increased. This is clearly observed in case $\Delta\sigma=0.35$ of the figure, where even after $N=1000$ cycles, neither ζ nor M_R have reached a stationary value.

The peculiar behavior of the system in the ratcheting regime allows for the characterization of the deformation state of the system through the strain rate and the resilient parameters. It is therefore crucial to know the influence of the confining pressure and the deviatoric stress on these parameters. For a complete review of the macroscopic factors affecting the resilient response of a granular material and some of the models proposed to account for it, we recommend Refs. [34] and [45].

To our knowledge, no systematic study has been carried out up to now elucidating the effect of the microscopic parameters of the system on the material reaction to cyclic loading, although they play an important role in it [46,47]. Combe *et al.* have identified contact stiffness and friction as the relevant microscopic parameters in this limit. Intergranular friction, in particular, appears then to be the dominating dissipative mechanism. The influence of contact stiffness and friction on the plastic behavior of a granular packing undergoing ratcheting will also be investigated in the following sections.

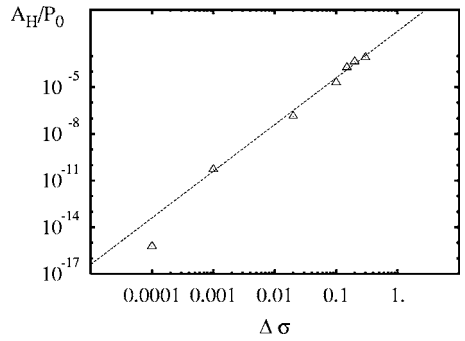

FIG. 7. Variation of the area enclosed by the stress-strain cycle A_H, for different values of $\Delta\sigma$. The area is scaled with the confining pressure. The dashed line shows the power law $y\propto x^3$. The data in the figure correspond to the simulation of a system with friction coefficient $\mu=0.1$, normal stiffness $k_n=1.6\times10^6$ N/m, tangential stiffness $k_t=0.33k_n$, and normal damping $1/\gamma_n=4\times10^3 t_s$. The confining pressure is $P_0=6\times10^{-3}k_n$ and the damping coefficient $\gamma_t=8t_s$.

V. HYSTERETICAL BEHAVIOR

History dependence is one of the most essential features of granular soils. In our simple model, we have shown the existence of hysteresis both in the shakedown and in the ratcheting regime. This has forced us to identify two different components to the total strain, namely the permanent and the resilient strain. In any stress cycle, the sliding contacts behave differently in the loading and unloading phase, leading to a different stiffness of the material in each of these phases. In this section, we are interested in the shape of the cycles and, more specifically, in its relationship with the evolution of the area closed by the strain-stress loop. If we assumed that the deformation in both spatial directions is approximately the same, this area is the dissipated energy within the cycle. This energy relaxes during the *post-compaction* from an initial high value to a constant value [23], reflecting the similarity of the hysteresis loops in the ratcheting regime (see Fig. 1). This final value is plotted in Fig. 7 for different deviatoric stress. A clear power-law behavior is observed in a wide range of values above the shakedown regime.

For the purposes that will be seen next, let us introduce the following dimensionless variables:

$$\gamma^* = \gamma_0 + \frac{\gamma_R}{2} - \gamma, \tag{16}$$

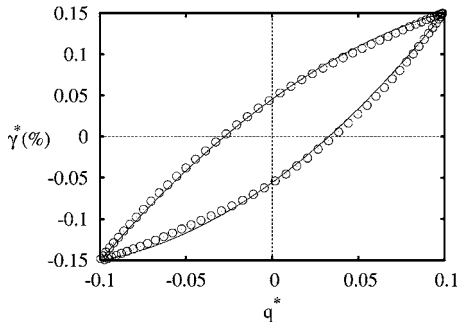

FIG. 8. Hysteresis stress-strain loop in the new variables γ^* and q^*. The solid points are the result of the simulation shown in Fig. 1 ($N=1000$). The solid lines are the best-fit to the expressions (19) and (18). The values of the constants for the theoretical lines are $B_L=0.04543$ and $B_U=0.05554$.

$$q^* = \frac{\Delta\sigma}{2} - \frac{\sigma_2 - \sigma_1}{P_0}, \tag{17}$$

where γ_0 is the permanent strain accumulated up to the end of the previous cycle we are interested in.

We express in Fig. 8 the limit cycle in Fig. 1 on these new variables. The best-fit curve to the points in the loading and unloading are also included. These curves can be expressed in the scaled variables,

$$\gamma_L^* = \frac{1}{M_R} q^* + B_L \left[\left(\frac{\Delta\sigma}{2} \right)^2 - q^{*2} \right], \tag{18}$$

in the loading, and

$$\gamma_U^* = \frac{1}{M_R} q^* - B_U \left[\left(\frac{\Delta\sigma}{2} \right)^2 - q^{*2} \right], \tag{19}$$

in the unloading phase. B_L and B_U are positive constants dependent of the confining pressure, but independent of the maximum deviatoric stress ($\Delta\sigma$). Note the use of the resilient parameter M_R in the previous expressions. From these formulas, it is then trivial to find the area of the cycle (A_H),

$$A_H = \oint \frac{\sigma_2 - \sigma_1}{P_0} d\gamma = \oint \gamma^* dq^* = \int_{-\Delta\sigma/2}^{\Delta\sigma/2} (\gamma_L^* - \gamma_U^*) dq^*$$
$$= (B_L + B_U) \left[\left(\frac{\Delta\sigma}{2} \right)^2 - \frac{\Delta\sigma}{3} \right]_{-\Delta\sigma/2}^{\Delta\sigma/2} = \frac{5(B_L + B_U)}{24} \Delta\sigma^3. \tag{20}$$

Due to our definition of q^* and γ^*, the area A_H is in fact the same as the area enclosed by the stress-strain cycle in Fig. 1. Our simple calculation explains the power-law behavior in Fig. 7 as a consequence of the nature of the stress-strain cycles obtained with our model. The explanation shown here somehow resembles the Rayleigh law for magnetization of ferromagnetic materials under low inductions [48]. Also in this case, the hysteresis energy loss (the area of the induction versus magnetization loop) behaves also like the cube of the induction. This power-law in ferromagnetic materials results from the quadratic dependence of the magnetic field on the magnetization. This is analogous to Eqs. (19) and (18) except for the fact that $B_L \neq B_U$, which reflects the asymmetry of the loops in the granular ratcheting regime. It is interesting to observe that the power law is identical to the one found for the dependence of the strain rate on the deviatoric strain, as shown in the previous section. In fact, the closed-loop approximation given by Eqs. (19) and (18) is not strictly valid in the limit $q^* \to 0$. The error of this quadratic approximation is of order $O(\Delta^3)$, and must be related to the cubic dependence of the strain accumulation on the load amplitude. A micromechanical explanation of this Rayleigh-like law in granular ratcheting is still an open issue.

In the ratcheting regime, the factors fulfill $B_U > B_L$. It is still to be determined which precise effect the behavior of the sliding contacts has on this observation. A better understanding of the nature of these constants and their dependences on the model parameters will help us to gain insight into the overall plastic response of the material.

VI. PERMANENT STRAIN ACCUMULATION

The influence of macromechanical magnitudes and the microscopic parameters of the model on the accumulation of permanent strain will be shown in this section. This will be done by measuring the strain rate in simulations where the confining pressure, the deviatoric stress, the friction coefficient, or the stiffness of the contacts is changed, while the rest of the parameters are kept fixed.

A. Influence of the confining pressure and deviatoric stress

Among all the possible parameters affecting the plastic behavior of a granular sample, the dependences on the confining pressure and on the deviatoric stress are known to be the most relevant ones [8]. Since P_0 is measured in units of the normal stiffness, $P_0 = \hat{P}_0 k_n$, there are two equivalent ways, in our model, of studying the effect of the confining pressure. On the one hand, the normal stiffness of the contact can be changed while maintaining the ratio k_t/k_n constant. On the other hand, the effective pressure $\hat{P}_0$ can be increased. In order to investigate the importance of the stress history of the sample, both methods have been used and the results are shown in Fig. 9(a). In each of the simulations, the system was first homogeneously compressed, and then subjected to cyclic loading. A power law relating the change of strain per cycle, $\Delta\gamma/\Delta N$, to P_0/k_n is found in a wide range of values. The best fit of the points leads to the linear behavior,

$$\frac{\Delta\gamma}{\Delta N} \propto \frac{P_0}{k_n}. \tag{21}$$

Dispersion of the data with respect to the empirical law in Eq. (21) is a direct consequence of the dependence of the final strain rate on the preparation of the material. Different confining pressures imply a different post-compaction process [23] and therefore a different density of the sample before cyclic loading. The range of densities involved in Fig. 9(a) goes from solid fractions $\Phi=0.82$ to $\Phi=0.9$. Our results show, in fact, that the strain rate seems to be much more sensitive to changes in the density than the resilient param-

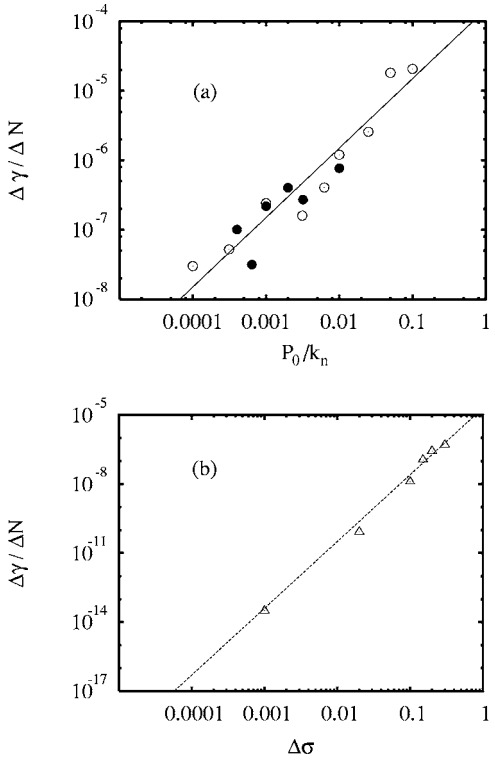

FIG. 9. Strain-rate dependence on the confining pressure, P_0, and the deviatoric stress $\Delta\sigma$. The solid line represents the best-fit power law. The simulation details are those of Fig. 7. (a) Data correspond to $\Delta\sigma=0.2$ and tangential damping $1/\gamma_t=8\times10^2t_s$. Solid circles were obtained keeping k_n constant and varying $\hat{P}_0$. The open circles, on the contrary, are the result of a series of simulations in which k_n was changed. The solid line on this graph shows a linear behavior. (b) Data correspond to $P_0=6\times10^{-3}k_n$ and $\gamma_t=8t_s$. The solid line represents the power law $y\propto x^3$. This is close to the power-law fitting in polygonal packing, whose exponent lies between 2.7 and 2.9 [1].

eters. This makes the investigation of the strain accumulation more difficult, limiting also the accuracy of our results on the relationship between the basic parameters of the system and the strain rate.

The history dependence of the material is not observed in part (b) of Fig. 9, where the strain rate accumulation is plotted versus the deviatoric stress for the same initial configuration of disks with solid fraction $\Phi=0.85$. The measures indicate a clear potential dependence of the strain rate with $\Delta\sigma$. Also a potential behavior (with exponent $m=2.8\pm0.1$) has been reported in a polygonal packing [1].

B. Influence of the micromechanical parameters

The strain-rate behavior as friction changes is slightly more complicated, if compared to the other parameters studied. For very low friction, no ratcheting is observed in the sample. Above a certain value of μ, however, a systematic ratcheting effect can be found. For the parameters used in the simulation shown in Fig. 10, this limit value is $\mu=0.05$. The strain rate is maximal at this friction, and (as observed in the figure) the strain rate decreases from this point, as friction is

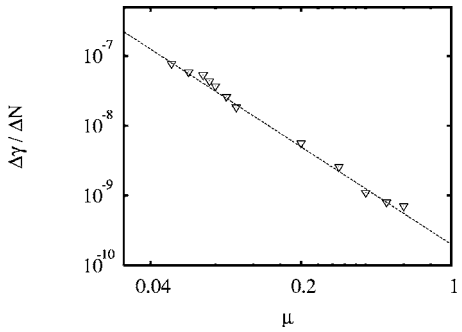

FIG. 10. Dependence of the strain rate on the friction coefficient μ. The data in the figure correspond to the simulation of a system normal stiffness $k_n=1.6\times10^6$ N/m, tangential stiffness $k_t=0.33k_n$, normal damping $1/\gamma_n=4\times10^3t_s$, and tangential damping $1/\gamma_t=8t_s$. The stress conditions are $P_0=10^{-3}\times k_n$ and $\Delta\sigma=0.1$. The solid fraction of the initial condition is $\Phi=0.93$. The solid line shows the law $y=x^{-2}$.

increased. The explicit dependence on the friction coefficient follows the power law,

$$\frac{\Delta\gamma}{\Delta N}\propto(\mu)^{-2.0\pm0.05}. \tag{22}$$

Figure 11 shows the variation of the permanent strain accumulation rate with the stiffness ratio for different samples prepared with the same confining pressure P_0 and normal stiffness k_n. A power-law behavior with a negative exponent is found. The best fit of the points of the figure gives

$$\frac{\Delta\gamma}{\Delta N}\propto\left(\frac{k_t}{k_n}\right)^{-0.3}, \tag{23}$$

indicating that stronger tangential forces produce a higher rate of the deformation.

An interpretation of these power-law relations could be done by exploring the statistical distribution of the contact forces and its evolution during the loading stage. An important parameter is the mobilized angle $\alpha=|f_t|/f_n$, which is bounded by the sliding condition $\alpha=\mu$. The statistical distri-

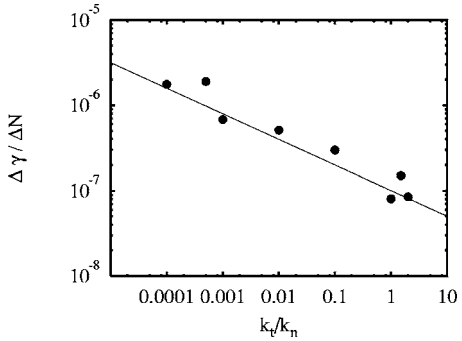

FIG. 11. Dependence of the strain rate on the stiffness ratio k_t/k_n. Data correspond to the simulation of a system with normal damping $1/\gamma_n=4\times10^3t_s$, tangential damping $1/\gamma_t=8\times10^2t_s$, solid fraction $\Phi=0.845\pm0.005$, and friction coefficient $\mu=0.1$. The stress conditions are kept constant, $P_0=10^{-3}\times k_n$ and $\Delta\sigma=0.2$. The solid line represents the power law $y\propto x^{-0.3}$.

bution of this variable is rather constant except for a peak at μ given by the sliding condition. The value of this peak depends on the friction coefficient. For small values of μ, a large number of contacts can reach the sliding condition so that the ratcheting response is expected to be large. For big values of μ, only a few contacts can reach the sliding conditions, which produces a small ratcheting response. A quantitative explanation for the power-law dependence will require us to calculate the evolution of the statistics of the sliding contacts and the contribution of the sliding to the global dissipation, but this is beyond the scope of this work.

VII. RESILIENT RESPONSE

Most theoretical models for the resilient response are based on curve-fitting procedures, using data from biaxial or triaxial tests. One of the most popular and earlier models is the so-called k-θ model [35], in which the resilient modulus is supposed to depend only on the mean stress θ,

$$M_r(\theta) = k\left(\frac{\theta}{\eta}\right)^n, \tag{24}$$

where k and n are material constants, η is a universal constant in units of stress (included for normalization), and θ is the absolute value of the first invariant of the stress tensor,

$$\theta \equiv |\mathrm{tr}(\hat{\sigma})|. \tag{25}$$

Many alternatives to and modifications of this model have been introduced, which are extensively used in practice [34,49,50]. One of the main restrictions of the k-θ model is the assumption of a constant Poisson ratio. Several studies have shown that the Poisson ratio is not a constant in the granular case, but varies with the applied stresses [36]. Another drawback of the model is that the effect of the deviatoric stresses on the resilient modulus is neglected. A straightforward modification of the k-θ model accounting for this latter restriction reads [37]

$$M_r(\theta, \Delta\sigma) = k\left(\frac{\theta}{\eta}\right)^n \left(\frac{\Delta\sigma}{\eta}\right)^m. \tag{26}$$

Note that, with respect to Eq. (24), a new material constant m has been introduced. In the simplest approximation, both exponents are assumed identical, $n \equiv m$ [38].

The validity of the k-θ model will be checked in this section. Note that, in the case of cyclic loading, given a fixed $\Delta\sigma$, the dependence of the resilient modulus on θ is similar to its dependence on P_0. Results will be shown on the influence of the confining stress and deviatoric stress on the resilient modulus and Poisson ratio. In the latter case, it will be particularly interesting to investigate the limit of validity of the common assumption of a constant Poisson ratio for granular matter.

A. Influence of the confining pressure

Figure 12 indicates that the k-θ model is in fact a very good approximation in the ratcheting regime for a wide range of pressures of P_0. The best fit to the empirical law of

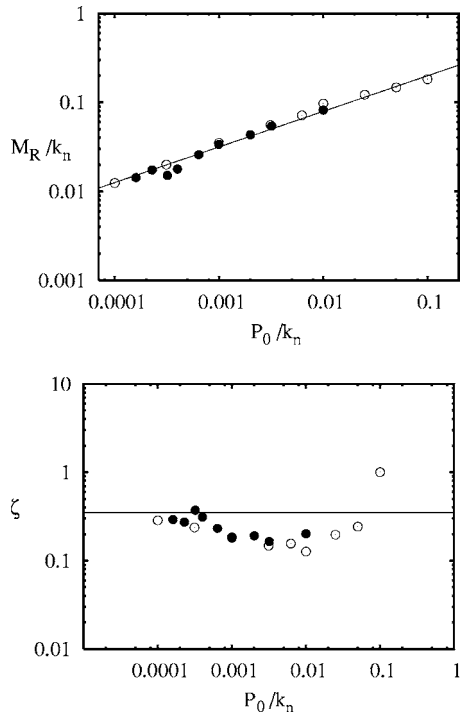

FIG. 12. Variation of the resilient parameters with the confining pressure P_0: resilient modulus M_R (top) and Poisson ratio ζ (bottom). The conditions of the simulation are the same as in Fig. 9. The line in the left plot is the best fit to the k-θ model. The solid line in the right figure is the value $\zeta = 0.35$, an estimation for the Poisson ratio of granular materials. The different symbols refer to two different methods explained in the text to study the influence of the confining pressure on the system.

Eq. (24) gives $n = 0.34 \pm 0.02$. This value agrees well with the experimental values in [36], where results on gravel show a power law with exponent $n = 0.31$.

Poisson ratio behaves in a completely different way. For low pressures, it decreases gradually as the pressure becomes higher. For $P_0 > 0.01 k_n$, however, there is a change in the trend, and ζ grows fast with P_0. This reflects a higher anisotropy of the deviatoric strain in systems compressed under a high pressure. Nevertheless, our results justify the use of a constant value of ζ in a first approximation, for a wide range of P_0, $10^{-4} k_n < P_0 < 10^{-2} k_n$. The most common estimate ($\zeta = 0.35$), however, slightly overestimates the values obtained in most of our simulations.

B. Influence of the deviatoric stress

Two stages are clearly distinguished in the behavior of the resilient parameters as a function of $\Delta\sigma$. For low values of the deviatoric stress, close to the shakedown regime, the resilient parameters remain approximately constant. The Poisson ratio remains closer to the indicated value $\zeta \approx 0.35$, which is the empirical fixed value usually assumed for unbound granular matter [36]. This value is shown in Fig. 13 with a solid line. For $\Delta\sigma > 0.1$, however, ζ shows a strong dependence on the deviatoric stress $\Delta\sigma$.

A simple empirical polynomial law is proposed in Ref. [36] for the dependence of ζ on the ratio of the deviatoric

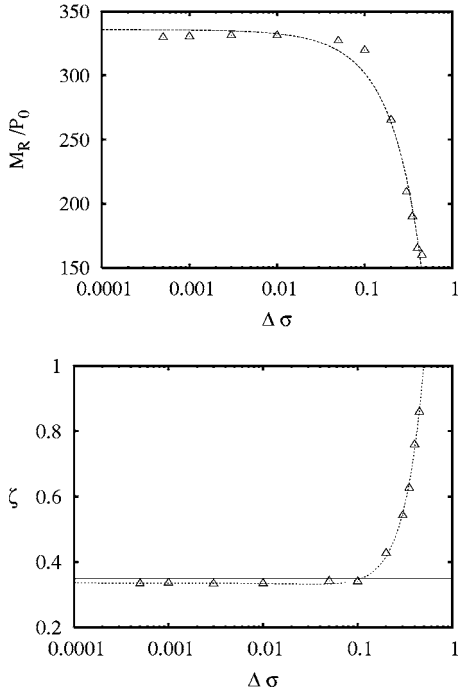

FIG. 13. Variation of the resilient parameters with the loading intensity $\Delta\sigma$. The simulation details are similar to those in Fig. 9 but with $k_n=2\times10^6$ N/m and $P_0=6\times10^{-4}k_n$. The best-fit curve to a second-order polynomial is plotted for the values of M_R in the top graph. In the bottom (Poisson ratio), the solid line corresponds to the value $\zeta=0.35$ and the dotted line to the best fit to equation $y(x)=a+bx+cx^2$ (details are given in the text).

and volumetric stresses. Although the range of values studied in this experiment is larger than the one presented here, our results confirm that the values of the Poisson ratio follow a second-order polynomial law on $\Delta\sigma$, where the best-fit curve is $\zeta=0.336(\pm0.001)-0.208(\pm0.001)\Delta\sigma+3.061(\pm0.001)\times(\Delta\sigma)^2$. This curve is plotted in the lower part of Fig. 13.

As opposed to the behavior of the Poisson ratio, the resilient modulus decreases as $\Delta\sigma$ increases. The dependence is also polynomial. In Fig. 13 (top), the curve $y(x)=335.7-316.8x+229.1x^2$ is plotted. Note that this result disagrees with the simplification of the generalized k-θ model ($m\equiv n$) of Eq. (26). The general law seems to be a better approximation in a wide range of values of the deviatoric stress, where the system shows neither collapse nor shakedown.

The dependence of the resilient parameters on the deviatoric stress results from the anisotropy induced in the contact network for large deviatoric loads. Near failure, a significant number of contacts are open in a direction perpendicular to the loading. This results in a smaller stiffness of the material as shown in the top of Fig. 13. The increase of the Poisson ratio in the bottom of this figure is a consequence of the formation of force chains, which enhances the anisotropy and leads to an increase of the effective Poisson ratio. A finer description of the effect of these force chains in the resilient response would require a detailed evaluation of the relation between the anisotropy of the contact network and the parameters of the anisotropic elasticity via fabric tensors [17,31].

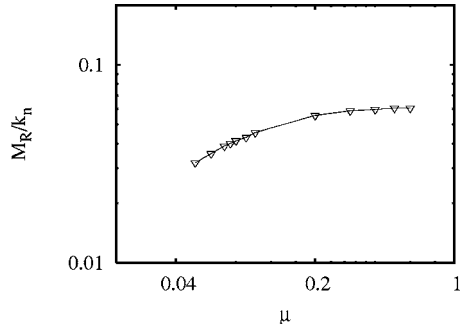

FIG. 14. Variation of the resilient modulus with the static friction coefficient μ. The conditions of the simulation are the same as in Fig. 10.

C. Influence of the micromechanical parameters

Figure 14 shows the change of the resilient modulus with friction. M_R grows for small frictions. However, the curve seems to reach a saturation level for frictions $\mu\approx0.4$.

Changing the ratio of contact stiffness (Fig. 15), a power-law dependence of M_R is observed for $k_t/k_n<0.1$, $M_R\propto(k_n/k_t)^{0.28}$, where the exponent is 0.28 ± 0.03. For stiffness ratios closer to unity $k_t/k_n\approx1$, the resilient modulus remains approximately constant or even decreases. The Poisson ratio also appears to be constant for $k_t<10^{-3}\times k_n$. Above $k_t/k_n=0.001$, ζ decreases to values below the reference value $\zeta=0.35$. For $k_t\geqslant k_n$, ζ starts growing again.

VIII. DISCUSSION AND FINAL REMARKS

A characterization of the material response in the granular ratcheting has been presented in terms of the strain rate, re-

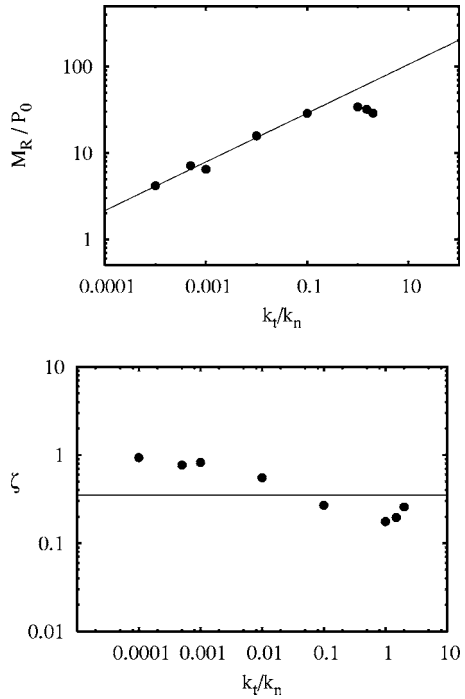

FIG. 15. Influence of the ratio of contact stiffness k_t/k_n on the resilient parameters. The details of the simulation are those of Fig. 11. The solid line shows a power law with exponent 0.28 in the top. The one at the bottom marks the value $\zeta=0.35$.

silient modulus, and the Poisson ratio. Studying the dependence of these parameters on the conditions of the biaxial test (stress configuration) and the main microscopic constants of the sample (friction and contact stiffness), we confirmed the persistence of the granular ratcheting in many different conditions and systems.

Given a compressed sample subjected to a biaxial test in which a cyclic loading is switched on, the system adapts to the new situation accumulating deformation and dissipating energy at a relatively high rate. After this *post-compaction* stage, the dissipated energy, both resilient moduli and the strain rate, reaches stationary values. The duration of the adaptation stage basically depends on the deviatoric stress, and is usually shorter for the resilient moduli than for the strain rate [23]. If the deviatoric stress is small enough, the perturbation introduced by the cyclic loading shakes down: The material adapts to the new situation so that there is no further accumulation of permanent strain. Above this limit, the material accumulates a certain amount of strain in each cycle. If the stress is below the collapse limit, the permanent strain accumulated after each cycle is constant. This is the so-called granular ratcheting, which has been described both experimentally [15,51] and in simulations [1,23].

Identical repetition of the strain-stress cycles is among the main characteristics of the granular ratcheting. This periodicity reflects the weak dependence of the resilient moduli on the stress history and, in the particular case of cyclic loading, on the number of applied cycles [8]. In all the simulations, a steady and stable resilient response is reached after some initial cycles. This kind of simple behavior is expected as long as the applied deviatoric stress remains below the collapse limit. Although many factors may influence the plastic response of the system, there is a simple characterization of the deformation in the ratcheting regime, in terms of the strain rate and the resilient moduli. This description takes advantage of the empirical fact that these magnitudes do not change in the ratcheting regime. We have investigated both micromechanical and macromechanical factors influencing the plastic response of the material, i.e., the dependence on the number of cycles, static friction, the confining pressure, the deviatoric stress, and the stiffness.

It was shown that the use of a constant Poisson ratio is a good approximation in most cases. It seems to be unsuitable, however, for very high confining pressures, very high deviatoric stresses, or for low values of the friction coefficient. The value for ζ estimated through our simulations would be slightly below the empirical value 0.35, assumed in many models of the resilient response of granular materials. This might be a consequence of the simplicity of the viscoelastic model, which does not include all the mechanisms involved in a real biaxial experiment.

M_R is a measure of the macroscopical stiffness of the material. Our results show that it is higher for strongly frictional materials. We also found that although preparing the sample with a higher confining pressure increases its stiffness, increasing the deviatoric stress reduces the stiffness of the packing.

Both the strain rate and the resilient modulus M_R show a power-law dependence with the confining pressure and the ratio of contact stiffness. The power law is similar for both magnitudes in the case of the confining pressure, but they have an opposite dependence on k_t/k_n. The dependence of M_R on the deviatoric stress is a second-order polynomial. The generalization of the k-θ model of Eq. (26) is not sufficient for our system, although Eq. (24) is a good approximation in many situations.

Reanalyzing our results on the strain rate, we can summarize them in the formal expression

$$\frac{\Delta\gamma}{\Delta N} \propto \frac{P_0}{\mu^2}(\Delta\sigma)^3\left(\frac{k_n}{k_t}\right)^{0.3}. \tag{27}$$

A direct relationship has been shown between this dependence, the power-law behavior of the dissipated energy per cycles as a function of the deviatoric stress imposed, and the systematic accumulation of permanent strain. Although the resilient parameters are not much affected by the stress history of the material, the strain rate is strongly dependent on it, therefore complicating the systematic investigation of the plastic response. In this context, it would be necessary to measure in more detail the influence of density and polydispersity on the possible shakedown of the material. The history dependence of the plastic response of the system is of vital importance to technical implications. Future topics for investigation also include the study of the shakedown-ratcheting transition as a function of the friction and the loading intensity. The influence of the system size, the dependence on the damping constants, and the effect of contact modeling on the material response are subjects of current work.

ACKNOWLEDGMENTS

The authors would like to thank Professor Deepak Dhar and Professor Ioannis Vardoulakis for very useful discussions. They also want to acknowledge the EU project Degradation and Instabilities in Geomaterials with Application to Hazard Mitigation (DIGA) in the framework of the Human Potential Program, Research Training Networks (HPRN-CT-2002-00220).

[1] F. Alonso-Marroquin and H. J. Herrmann, Phys. Rev. Lett. **92**, 054301 (2004).

[2] P. Reimann, Phys. Rep. **361**, 57 (2002).

[3] I. Zapata, R. Bartussek, F. Sols, and P. Hänggi, Phys. Rev. Lett. **77**, 2292 (1996).

[4] J. Howard, Nature (London) **389**, 561 (1997).

[5] K. Svoboda, C. F. Schmidt, B. J. Schnapp, and S. M. Block, Nature (London) **365**, 721 (1993).

[6] K. Kitamura, K. Tokunaga, M. Iwane, and T. Yanagida, Nature (London) **397**, 129 (1999).

[7] P. H. Dybvig, Rev. Econ. Stud. **62**, 287 (1995).
[8] F. Lekarp, A. Dawson, and U. Isacsson, J. Transp. Eng. **126**, 76 (2000).
[9] G. Royer-Carfagni, in *Novel Approaches in Civil Engineering* (Springer-Verlag, Berlin, 2004), pp. 177–185.
[10] M. Huang, Z. Suo, Q. Ma, and H. Fujimoto, J. Mater. Res. **15**, 1239 (2000).
[11] G. L. England, T. D. C. M. Tsang, N. Mihajlovic, and J. B. Bazaz, in *Static and Dynamic Properties of Gravelly Soils*, edited by M. D. Evans and R. J. Fragaszy (ASCE, 1995), pp. 64–76.
[12] J. Burland and C. Viggiani, Riv. Ital. Geotec. **28**, 179 (1994).
[13] F. Lekarp and A. Dawson, Constr. Build. Mater. **12**, 9 (1998).
[14] R. W. Sharp and J. R. Booker, J. Transp. Eng. **110**, 1 (1984).
[15] S. Werkmeister, A. R. Dawson, and F. Wellner, J. Transp. Res. Board **1757**, 75 (2001).
[16] P. A. Cundall, Ing.-Arch. **59**, 148 (1989).
[17] S. Luding, Int. J. Solids Struct. **41**, 5821 (2004).
[18] M. Oda, K. Iwashita, and H. Kazama, in *IUTAM Symposium on Mechanics of Granular and Porous Materials* (Kluwer Academic Publishers, Dordrecht, 1997), pp. 353–364.
[19] F. Radjai, M. Jean, J. J. Moreau, and S. Roux, Phys. Rev. Lett. **77**, 274 (1996).
[20] J. J. Moreau, Eur. J. Mech. A/Solids **13**, 93 (1994).
[21] C. Coste, Phys. Rev. E **70**, 051302 (2004).
[22] Z. Farkas, F. Szalai, D. E. Wolf, and T. Vicsek, Phys. Rev. E **65**, 022301 (2002).
[23] R. García-Rojo and H. Herrmann, Granular Matter **7**, 109 (2005).
[24] D. Kolymbas, *Introduction to Hypoplasticity* (Balkema, Amsterdam, 1999).
[25] F. Tatsuoka, T. Masuda, M. S. A. Siddiquee, and J. Koseki, J. Geotech. Geoenviron. Eng. **129**, 450 (2003).
[26] Y. Mroz, F. Norris, and G. Zienkiewicz, Geotechnique **31**, 451 (1981).
[27] A. Niemunis and I. Herle, Mech. Cohesive-Frict. Mater. **2**, 279 (1996).
[28] Y. F. Dafalias, J. Eng. Mech. **112**, 966 (1986).
[29] C. Thornton and D. J. Barnes, Acta Mech. **64**, 45 (1986).
[30] S. C. Cowin, Mech. Mater. **4**, 137 (1985).
[31] F. Alonso-Marroquin, S. Luding, H. J. Herrmann, and I. Vardoulakis, Phys. Rev. E **71**, 051304 (2005).
[32] J. A. Astrom, H. J. Herrmann, and J. Timonen, Phys. Rev. Lett. **84**, 638 (2000).
[33] M. Lätzel, S. Luding, H. J. Herrmann, D. W. Howell, and R. P. Behringer, Eur. Phys. J. E **11**, 325 (2003).
[34] F. Lekarp, U. Isacsson, and A. Dawson, J. Transp. Eng. **126**, 66 (2000).
[35] R. G. Hicks and C. L. Monismithi, Highw. Res. Rec. **345**, 15 (1971).
[36] J. J. Allen, Transp. Res. Rec. **510**, 1 (1974).
[37] J. Uzan, Transp. Res. Rec. **1022**, 52 (1985).
[38] W. A. Tam and S. F. Brown, in *Urban Traffic Control Workshop*, 14th ARRB Conference, Australia, 1988, Vol. 14, pp. 155–163.
[39] P. A. Cundall and O. D. L. Strack, Geotechnique **29**, 47 (1979).
[40] M. P. Allen and D. J. Tildesley, *Computer Simulation of Liquids* (Oxford University Press, Oxford, 1987), Chap. Appendix E, pp. 340–342.
[41] C. S. Desai and H. J. Siriwardane, *Constitutive Equations for Engineering Materials* (Prentice-Hall, Englewood Cliffs, NJ, 1984).
[42] I. Vardoulakis and J. Sulem, *Bifurcation Analysis in Geomechanics* (Blakie Academic & Professional, London, 1995).
[43] F. Radjai and S. Roux, Phys. Rev. Lett. **89**, 064302 (2002).
[44] I. Vardoulakis, Ing.-Arch. **59**, 106 (1989).
[45] E. Taciroglu and D. Hjelmstad, J. Eng. Mech. **128**, 969 (2002).
[46] G. Combe and J.-N. Roux, C. R. Phys. **3**, 131 (2002).
[47] G. Combe and J.-N. Roux, Phys. Rev. Lett. **85**, 3628 (2000).
[48] S. Zapperi, G. Durin, and A. Magni, J. Magn. Magn. Mater. **242-245**, 987 (2002).
[49] K. D. Hjemlstad and E. Taciroglu, J. Eng. Mech. **126**, 821 (2000).
[50] A. Nataatmadjai and Y. L. Tan, J. Transp. Eng. **127**, 450 (2001).
[51] S. Werkmeister, A. R. Dawson, and F. Wellner, Str. Autob. **1**, 1 (2004).
[52] C. Thornton, Geotechnique **50**, 43 (2000).
[53] L. Brendel and S. Dippel, in *Physics of Dry Granular Media*, edited by H. J. Herrmann, J.-P. Hovi, and S. Luding (Kluwer Academic Publishers, Dordrecht, 1998), p. 313.